International Journal of Nanomedicine

Dovepress
open access to scientific and medical research

Open Access Full Text Article

ORIGINAL RESEARCH

# Amino-Functionalized Nitrogen-Doped Graphene Quantum Dots for Efficient Enhancement of Two-Photon-Excitation Photodynamic Therapy: Functionalized Nitrogen as a Bactericidal and Contrast Agent

This article was published in the following Dove Press journal:
*International Journal of Nanomedicine*



Wen-Shuo Kuo[1,2,*]
Tien-Sung Yeh[3,*]
Chia-Yuan Chang[4]
Jui-Chang Liu[2]
Chang-Hsin Chen[5]
Edmund Cheung So[6,7]
Ping-Ching Wu[8]

[1]School of Chemistry and Materials Science, Nanjing University of Information Science and Technology, Nanjing 210044, Jiangsu, People's Republic of China; [2]Allergy & Clinical Immunology Research Center, National Cheng Kung University Hospital, College of Medicine, National Cheng Kung University, Tainan 701, Taiwan, Republic of China; [3]Department of Physical Medicine and Rehabilitation, An Nan Hospital, China Medical University, Tainan 709, Taiwan, Republic of China; [4]Department of Mechanical Engineering, National Cheng Kung University, Tainan 701, Taiwan, Republic of China; [5]AbVision Inc., Milpitas, CA 95035, USA; [6]Department of Anesthesia & Medicine Research, An Nan Hospital, China Medical University, Tainan 709, Taiwan, Republic of China; [7]Graduate Institute of Medical Sciences, Chang Jung Christian University, Tainan 711, Taiwan, Republic of China; [8]Department of Biomedical Engineering, National Cheng Kung University, Tainan, 701, Taiwan, Republic of China

*These authors contributed equally to this work

Correspondence: Edmund Cheung So; Ping-Ching Wu
Email edmundsotw@gmail.com; wbcxyz@bme.ncku.edu.tw

**Background:** Although graphene quantum dots (GQDs) have received considerable research attention for their applications in various fields, the use of GQDs, such as nitrogen-doped GQDs (N-GQDs) and amino-functionalized N-GQDs (amino-N-GQDs), as photosensitizers to facilitate photodynamic therapy (PDT) has received limited research intention. To address this research gap, this study prepared novel amino-N-GQDs and investigated their properties.

**Methods:** The amino-N-GQDs subjected to two-photon excitation (TPE) exhibited remarkable bactericidal capability in PDT. The bonding compositions of nitrogen and the amino-functionalized group played a critical role in their antimicrobial effects.

**Results:** Compared with amino-group-free N-GQDs and amino-N-free GQDs, the amino-N-GQDs generated a higher amount of reactive oxygen species, demonstrating their superior efficacy for two-photon PDT. Additionally, the intrinsic luminescence properties and high photostability of the amino-N-GQDs demonstrate their suitability as an effective two-photon contrast agent for tracking bacteria during two-photon biomedical imaging.

**Conclusion:** The amino-N-GQD and their remarkable properties may provide an efficient alternative approach for observing and easily eliminating malignant microbes in the future.

**Keywords:** nitrogen atom-doped graphene quantum dots, amino-functionalized and nitrogen atom-doped graphene quantum dots, two-photon photodynamic therapy, two-photon contrast agent, two-photon biomedical imaging

## Introduction

In multiphoton microscopy, which is also referred to as TPE laser scanning microscopy, fluorescence is created through nonlinear localized excitations. This method has been extensively used in imaging research.[1] In bioimaging applications, multiphoton microscopy is generally coupled with near-infrared (NIR) laser excitation to ensure maximal tissue transmission. NIR laser excitation is characterized by low energy absorption, a low degree of scattering, minimal photobleaching, and optimal irradiation penetration, thus enabling the observation of thick tissues and deep biological specimens. Furthermore, multiphoton microscopy has been helpful in therapies involving photoexcitation.[2] Multiphoton microscopy involves a short photoexcitation period

and has ultralow energy requirements; therefore, it has potential applicability in PDT. In PDT, reactive oxygen species (ROS) are formed through the reaction of molecular oxygen with a photosensitizer that has been photoexcited by light of an appropriate wavelength and energy. Singlet oxygen $^{1O2}$ and superoxide radical anions ($O_2^{\cdot -}$) typically constitute PDT-generated ROS. These species can irreversibly damage cells because they undergo oxidative reactions with the neighboring biological substrates. To achieve efficient PDT, obtaining a photosensitizer with a large TPE cross section is crucial; however, some photosensitizers are toxic and should not be employed. A large cross section is particularly crucial for molecular activity and photoproperty evaluation using two-photon techniques. When a large cross section is used, the proportion of specimen-absorbed input energy is high, which reduces the likelihood of photodamage. Accordingly, a large TPE cross section renders a photosensitizer efficient for nonlinear microscopic investigations.[3]

Materials with two-photon properties have received considerable attention because of their potential utility in PDT and bioimaging applications.[1] Several novel TPE materials are based on graphene,[4] a two-dimensional hexagonal-lattice monolayer comprising graphite and carbon atom bonds. Graphene-based materials have been investigated in numerous fields. When such materials are combined with photosensitizers, PDT mechanisms can be induced.[5] In a previous study, ROS were generated directly using GQDs as a photosensitizer.[6] The main limitation of the aforementioned study is that it did not consider PDT involving two-photon processes. GQDs can be illuminated by surface groups, a process that could be among potential photoluminescence (PL)-based mechanisms underlying intrinsic- and defective state emissions.[7]

In semiconductors, doping has a critical effect because it can substantially alter the carrier density, resulting in distinct optical and electrical properties. Nitrogen functionalization and doping are thus considered to be highly useful because they alter the intrinsic properties of GQDs. The five valence electrons and electron-donating N atoms of GQDs, whose atomic size is comparable to that of carbon atoms, provide a high positive charge density to the adjacent carbon atoms in graphene. Therefore, because of the remarkable edge and quantum confinement effects of GQDs, N-atom-doped GQDs (N-GQDs) have improved electrochemical, electrocatalytic, and photochemical activities, which can be advantageous for biomedical and optoelectronic applications. Moreover, achieving amino group functionalization through chemical modification with primary amine molecules leads to strong electron donation, which has a considerable influence on the electronic properties of N-GQDs.[8] Because of the amino-functionalized N-GQDs (amino-N-GQDs), intersystem crossing can be effectively achieved; this is because intersystem crossing competes with internal conversion among states with the same multiplicity, which results in simultaneous PL and ROS generation in PDT.[9]

In the present study, N-GQDs exhibited superior two-photon properties to N-free GQDs. We noted that the N dopant demonstrated remarkable bactericidal capability in two-photon PDT and that amino group functionalization played a critical role in the antimicrobial effects of the N-GQDs. This functionalization also enhanced the effectiveness of the N-GQDs as contrast agents when compared with amino-group-free N-GQDs. Furthermore, we explored the two-photon properties of GQD-based materials—GQDs, N-GQDs, and amino-N-GQDs—through TPE microscopy in the NIR spectrum. A previous study reported that strong electron donation and a large π-conjugated system could improve charge transfer efficiency in amino-N-GQDs;[10] this could result in enhanced two-photon absorption (TPA), post-TPE stability, TPE cross sections, and two-photon luminescence (TPL), in addition to engendering a relatively high radiative–to–nonradiative decay rate ratio. Additionally, the N-GQDs exhibited a relatively short lifetime, demonstrating their potential for use as bactericidal and contrast agents in biomedical imaging and biomedical tracking. In this study, the prepared amino-N-GQDs were used as two-photon photosensitizers to localize or track analytes that were subjected to amino-N-GQD treatment under TPE at an excitation energy of 394.24 nJ pixel$^{-1}$ and laser power of 3.9424 mW (refer to the Supplementary Information for details about the laser power calculations); as illustrated in Figure 1, the laser system's x−y focal point and z-axis resolution were 0.37538 and 0.90265 mm, respectively. The analytes were eliminated completely through TPE (800 nm) after 700 scans (total effective exposure time, 3.171 s; scan rate, 4.53 ms scan$^{-1}$; scan area, 200 μm × 200 μm; refer to the Supplementary Information for the calculations). This finding indicates that the PDT was highly efficient and that the amino-N-GQDs had a higher elimination efficiency than did the amino-group-free N-GQDs and amino-N-free GQDs (~58% and ~35% elimination, respectively). Under TPE mediation, the amino-N-GQDs had more favorable luminescence and stability than did the other two GQD-based materials. Accordingly, in a three-dimensional (3D) environment, effective tracking or localization of amino-N-GQD-treated

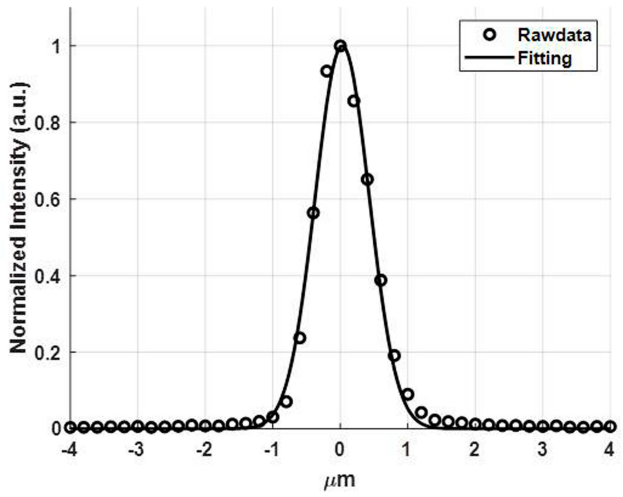


**Figure 1** According to the z-axis scan of a gold thin film for measuring the signal of second harmonic generation at different positions, the z-axis resolution of the laser system (full width at half maximum) was 0.90265 μm (fitting performed using the Gaussian function).

analytes can be achieved using amino-N-GQDs as a two-photon contrast agent. In combination with two-photon PDT, the amino-N-GQDs efficiently killed the entirety of the bacteria under observation.

# Materials and Methods

## Bacterial Cultures

*Bacillus subtilis* (*B. subtilis*) obtained from our own laboratory were grown in nutrient agar of Luria-Bertani (LB) broth (per liter: tryptone 10g, yeast extract 5g, sodium chloride 10g, agar 15g, and pH tuned to 7.5) (Sigma Aldrich Co., St Louis, MO, USA) and incubated at 37 °C.

## Biocompatibility Assay with Colony-Forming Unit (CFU) Counting Method

*B. subtilis* ($OD_{600}$ ~0.05) was added with material-$Ab_{TasA}$ (6 μg $mL^{-1}$) by incubating for 3 h at 37 °C. After incubation, the mixture was centrifuged and the pellets of bacteria were diluted ($OD_{600}$ ~0.05). Then, a dilution factor in the range of $10^{-5}$ to $10^{-8}$ was used for the incubated bacteria with plating on the agar plates. The plates were placed overnight in an incubator at 37 °C. The number of surviving bacteria was determined and expressed as a percentage (%) that corresponds to the unit of CFU $mL^{-1}$ after incubation. Data are means ± SD (n=6)

All material and methods for this article can be found in the Supplementary Information.

# Results and Discussion

## Characterization of GQD-Based Materials

The amino-N-GQDs were prepared through ultrasonic shearing. The shearing reaction involved a graphene oxide sheet that was obtained using a modified Hummers method.[11] High-resolution transmission electron microscopy (HR-TEM) was used to obtain the mean lateral size of the quantum dots under high magnification. The results revealed that mean lateral size of the quantum dots was 7.1 ± 0.6 nm. Favorable crystallinity and lattice distance were observed, which could be attributed to the d-spacing of the graphene $\{1\bar{1}00\}$ lattice fringes (Supplementary Information, Figure S1A). Dynamic light scattering was conducted to determine the size distribution of the GQDs, and the results are presented in Table S1 (Supplementary Information). The height profiles of the GQDs were determined through atomic force microscopy (AFM), and the results indicated a single 1.08 ± 0.03-nm-thick layer of amino-N-GQDs (Supplementary Information, Figure S1B). Figure S1C (Supplementary Information) presents the X-ray diffraction (XRD) spectrum derived through crystallinity analysis. The diffraction angle ($2\theta$) of the amino-N-GQD material was nearly 24.3°, indicating that the material had appropriate layer regularity and a well-ordered lamellar structure with an interlayer distance of 0.360nm. The interfringe distances were 0.213 and 0.360 nm, which could be attributed to graphite's in-plane lattice spacing and basal plane distance, respectively. Moreover, the values observed for the amino-N-GQDs are consistent with those reported in the literature (0.340–0.403 nm).[12,13] The XRD results also indicated that the basal plane was not considerably functionalized. This finding is in agreement with the theories that graphene has considerably more active edges than in-plane carbons do and that functional groups are present at the amino-N-GQD edges.[13] The large basal spacing of the amino-N-GQD material can be attributed to the accommodation of several oxygen species, such as epoxy, hydroxyl, and amino groups, and the alteration of the carbon hexahedron grid plane, which resulted in increased graphene layer spacing. Raman spectroscopy was conducted for the GQDs. In the derived Raman spectrum, the integrated intensity ratio of the D-band (~1384$cm^{-1}$) to the G-band (~1607 $cm^{-1}$)—that is the $I_D/I_G$ ratio—was approximately 0.88 (Supplementary Information, Figure S1D). The $I_D/I_G$ ratio was used in Raman spectroscopy to estimate the

mean $sp^2$ domain size of the GQD-based specimens. The size obtained from the Raman estimation (~7.0 nm) approximately matched that obtained from HR-TEM; nevertheless, the value obtained from the Raman estimation was slightly lower than that obtained from HR-TEM because oxygenated regions were ignored in the Raman estimation[14] (Supplementary Information, Equations S4 and S5). An absorption peak was observed at approximately 221 nm, corresponding to the π–π* transition of aromatic C=C bonds. Furthermore, a peak was observed at nearly 324 nm and was attributed to n–π* transitions of the C–N and C=O shoulders, indicating the occurrence of a π electron transition in the oxygen-containing amino-N-GQDs and confirming the N doping of the dots, as revealed through ultraviolet (UV)–visible (Vis) spectroscopy (Supplementary Information, Figure S1E). X-ray photoelectron spectroscopy (XPS) was applied to investigate the surface chemistry of the amino-N-GQDs, which were predominantly composed of carbon and nitrogen atoms. The C(1s) spectra were deconvoluted, and the corresponding peaks were fitted with a Gaussian function. The results revealed the presence of nonoxygenated rings (C–C/C=C, 286.0 eV), C–N bonds (286.7 eV), hydroxyl groups (C–O, 287.0 eV), and carbonyl groups (C=O, 288.3 eV) (Supplementary Information, Figure S1F). We also used the Gaussian function to fit the N(1s) spectra. The results indicated the presence of pyridinic N (398.3 eV), amino N ($NH_2$, 399.0 eV), pyrrolic N (399.7 eV), quaternary N (400.5 eV), and amide N (O=C–N, 401.3 eV) compounds (Supplementary Information, Figure S1G). The table in Figure S1 (Supplementary Information) presents a summary of the bonding compositions and atomic ratios of the amino-N-GQDs. The atomic ratio of O(1s) to C(1s) and that of N(1s) to C(1s) were 28.2% and 4.5%, respectively. Fourier-transform infrared spectroscopy was also executed to identify exposed functional groups on the amino-N-GQDs, and Figure S2 (Supplementary Information) displays the results. On the basis of the aforementioned characterization results, the preparation of the amino-N-GQDs was successful.

## Identification of the Generated ROS

ROS induce DNA damage, inactivate enzymes, and oxidize amino acids, all of which engender bacterial injury. $^1O_2$ and $O_2.^-$ are ROS with major roles in PDT. Therefore, $^1O_2$ and $O_2.^-$ produced after laser irradiation of amino-N-GQDs should be directly detected. Accordingly, this study conducted PDT under the following conditions: the excited triplet amino-N-GQDs were combined with oxygen and then illuminated with light of suitable wavelength and energy; Singlet Oxygen Sensor Green (SOSG) reagent, trans-1-(2′-methoxyvinyl)pyrene (*t*-MVP), 2,3-bis (2-methoxy-4-nitro-5-sulfophenyl)-2H-tetrazolium-5-carboxanilide (XTT), and glutathione (γ-L-glutamyl-L-cysteinyl-glycine, GSH) were subsequently introduced.[12,15-17] To capitalize on the potential bactericidal capability of the amino-N-GQDs, we determined their optimal wavelength. The maximum TPA ratio of the amino-N-GQDs was observed at approximately 800 nm, which was thus considered the most efficient wavelength under TPE (Figure 2A); this could be attributed to the interband transitions. Hence, we used 800 nm as the wavelength in subsequent experiments. The amino-N-GQDs were photoexcited through TPE (power, 394.24 nJ $pixel^{-1}$; number of scans, 700; exposure wavelength, 800 nm; total effective exposure time, ~3.171 s) with a delivered dose of 6 μg $mL^{-1}$ (Supplementary Information, Table S2). To verify that ROS were involved in the PDT effect of the amino-N-GQDs, we used α-tocopherol for ROS neutralization.[13] This step reduced the quantity of the generated ROS, and we discovered an increase in cell viability, as expected. Inadvertent exposure of the amino-N-GQDs to white light would have led to the production of $^1O_2$ and $O_2.^-$, which would have compromised our experimental results;[18] to prevent this, the subsequent PDT-related experiments were conducted in the dark. We considered the quantities of $^1O_2$ and $O_2.^-$ generated to be critical. According to the experimental results, the amino-N-GQDs exhibited strong antibacterial effects, demonstrating their potential for application in PDT. We observed that after the GQD-based materials were subjected to the same experimental conditions, the amino-group-free N-GQDs (ie, N-GQDs) and amino-N-free GQDs (ie, GQDs) demonstrated a lower capability to generate $^1O_2$ and $O_2.^-$ (Supplementary Information, Figures S3 and S4) than did the amino-N-GQDs (Supplementary Information, Table S2). Specifically, the amino-N-GQDs generated larger quantities of $^1O_2$ and $O_2.^-$ than did the N-GQDs and GQDs. We obtained an estimated singlet oxygen quantum yield ($\psi_\Delta$) of 0.55 for the amino-N-GQDs, 0.46 for the N-GQDs, and 0.31 for the GQDs (for reference, $\psi_\Delta$ = 0.64 for meso-tetra(4-sulfonatophenyl)porphine dihydrochloride dissolved in $D_2O$[19]).

## Antimicrobial Effects Under TPE

TasA is the primary protein component of the biofilm extracellular matrix of *B. subtilis*, a Gram-positive

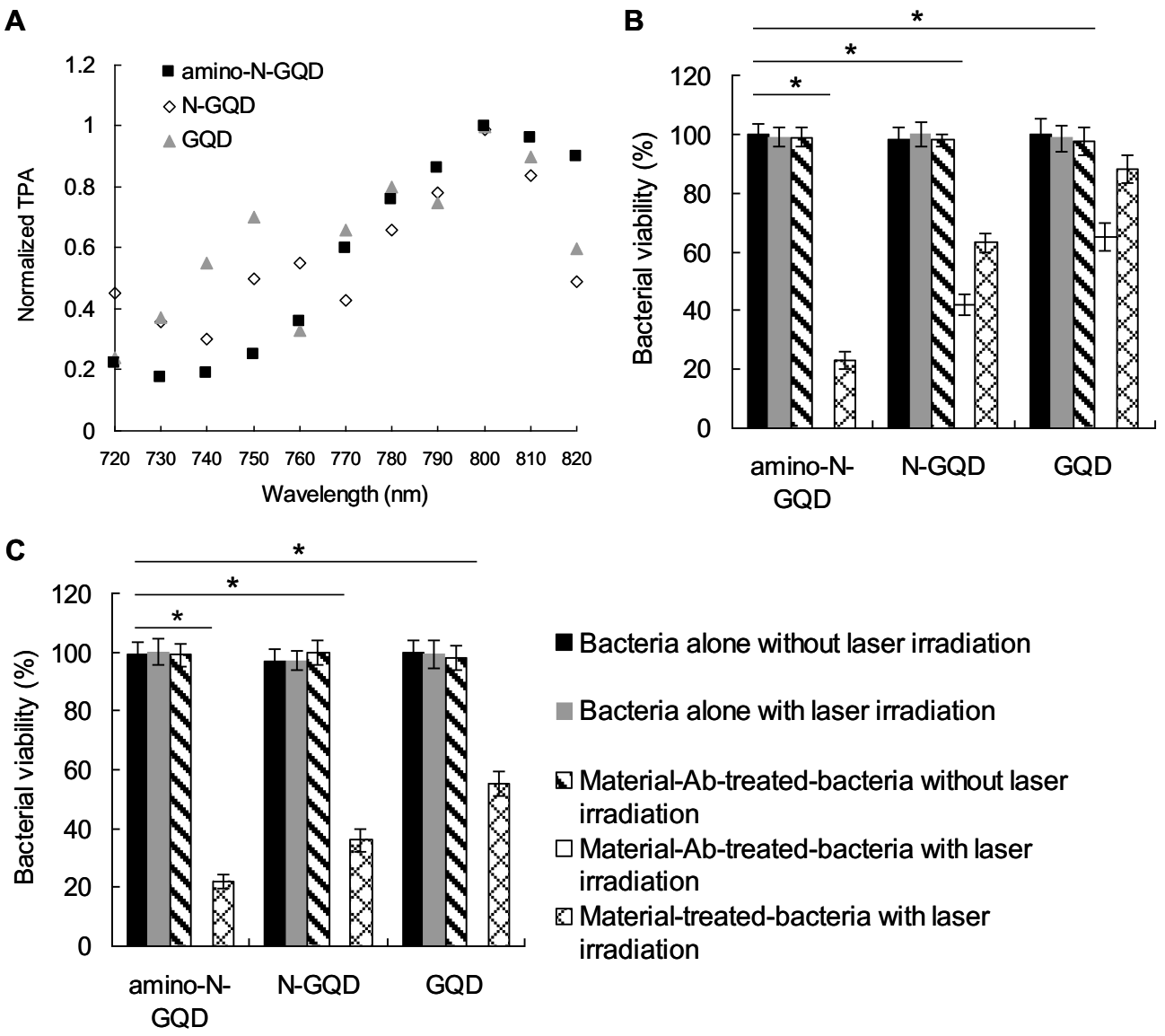


**Figure 2** (**A**) Relative TPA spectra of materials. Signals were observed through TPE at various wavelengths (720–820 nm) at 98.56 nJ pixel$^{-1}$. (**B**) Viability (%), which was quantified following the number of material–$Ab_{TasA}$-treated *B. subtilis* found to be viable using the CFU assay at a TPE power of 394.24 nJ pixel$^{-1}$ (scanning frequency, 700 scans; total effective exposure time, ~3.171 s; Ex, 800 nm). Regarding the amino-N-GQD-, N-GQD-, and GQD-$Ab_{TasA}$-treated *B. subtilis* subjected to TPE, $p < 0.0001$, $p = 0.0583$, and $p = 0.6227$, respectively. (**C**) CFU assays for amino-N-GQD-, N-GQD-, and GQD-Ab-treated bacteria were conducted at power levels of 394.24, 475.20, and 566.72 nJ pixel$^{-1}$, respectively (scanning frequency, 700 scans; total effective exposure time, ~3.171 s; Ex, 800 nm). For all material–$Ab_{TasA}$-treated *B. subtilis* subjected to TPE, $p < 0.0001$. Delivered dose: $OD_{600}$~0.05 of *B. subtilis* and 6 μg mL$^{-1}$ material–$Ab_{TasA}$. Data are means ± SD (n = 6). *$p$ value obtained by Student's $t$-test.

bacterium. To explore antimicrobial effects, we used *B. subtilis* as the experimental template. To improve the efficiency and specificity of TasA, one of the quantum dot materials was coated onto $Ab_{TasA}$ to form material–$Ab_{TasA}$. We determined the antimicrobial potential of the amino-N-GQD, N-GQD, and GQD materials by conducting PDT experiments against *B. subtilis* ($OD_{600}$: 0.05) at a TPE power of 394.24 nJ pixel$^{-1}$ (number of scans, 700; total effective exposure time, ~3.171 s; wavelength, 800 nm) and material dose of 6 μg mL$^{-1}$. The system was incubated in the dark for 3h at 37°C. We calculated the number of surviving bacteria (in colony-forming units per milliliter, CFU mL$^{-1}$) and express it as a percentage (%) herein. We observed that the materials subjected to laser exposure and those not subjected to laser exposure had no bactericidal effects on *B. subtilis* when used alone (Figure 2B). However, under TPE, the amino-N-GQDs completely eliminated the bacteria (100% elimination), demonstrating their efficient antibacterial effect. Next, we investigated whether the N-bonding composition and amino-functionalized group would affect bacterial viability. We conducted identical photoexcitation experiments

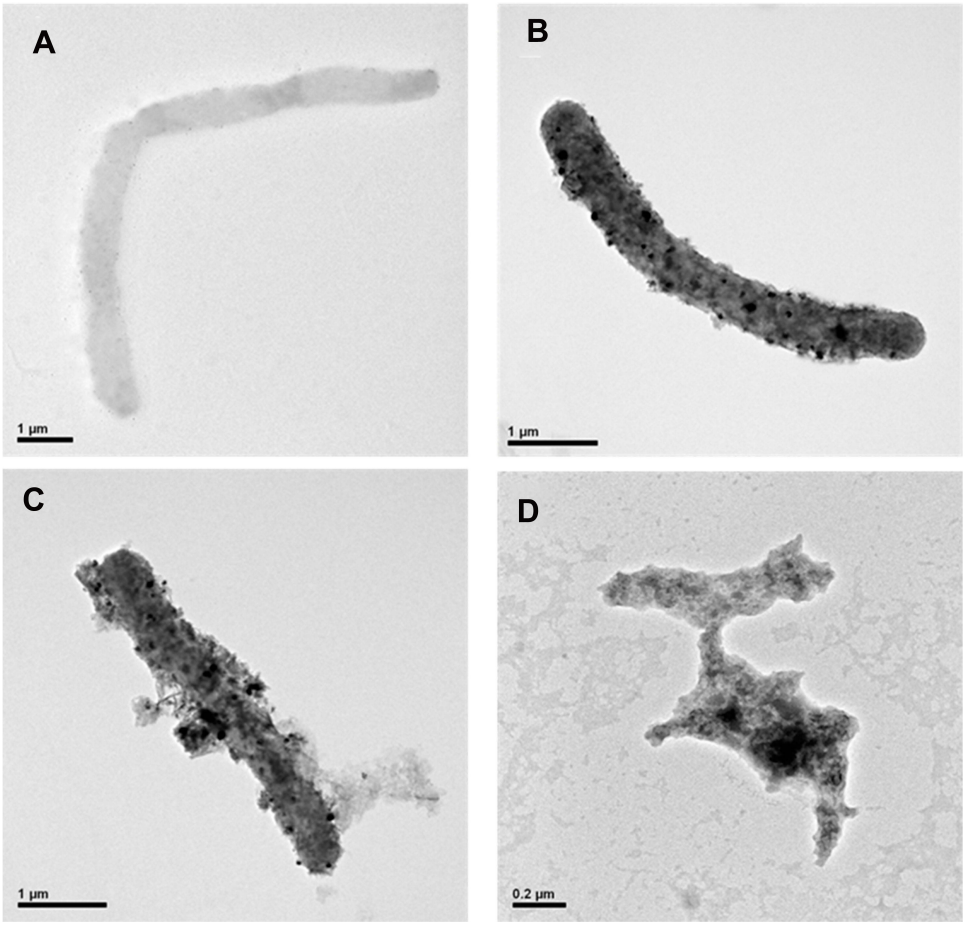


**Figure 3** TEM images showing (**A**) bare *B. subtilis*. (**B**) Bacteria treated with amino-N-GQD–$Ab_{TasA}$ and incubated for 3 h, and (**C**) 3 days of incubation, respectively. (**D**) The photoexcited amino-N-GQD–$Ab_{TasA}$-treated-*B. subtilis* for 3 h of incubation with 394.24 nJ $pixel^{-1}$ TPE (scanning frequency, 700 scans; total effective exposure time, ~3.171 s; Ex, 800 nm). Delivered dose: $OD_{600}$~0.05 of *B. subtilis* and 6 μg $mL^{-1}$ material–$Ab_{TasA}$.

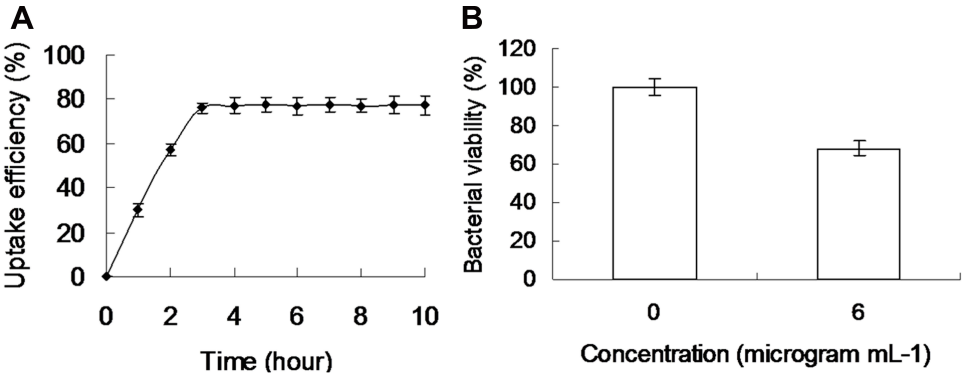


**Figure 4** (**A**) Uptake assay results derived for *B. subtilis* treated with amino-N-GQD–$Ab_{TasA}$ for 0–10 h at 37°C. (**B**) Viability (%), which was quantified following the number of amino-N-GQD–$Ab_{TasA}$-treated *B. subtilis* found to be viable using the CFU assay. Delivered dose: $OD_{600}$~0.05 of *B. subtilis* and 6 μg $mL^{-1}$ material–$Ab_{TasA}$. Data are means ± SD (n = 6).

and discovered that the N-GQDs had a weaker bactericidal effect than did the amino-N-GQDs (Figure 2B). The viability of the N-GQD–$Ab_{TasA}$-treated *B. subtilis* cells was 42% after exposure, which corresponded to a nearly 0.382 log10 reduction (Supplementary Information, Figure S3). We also found that regardless of the type of GQD-based material, the bactericidal effect of the amino-N-GQDs on *B. subtilis* was stronger than those of N-GQD–$Ab_{TasA}$ and

GQD–$Ab_{TasA}$ (65% bacterial viability, ~0.189 log10 reduction; Supplementary Information, Figure S3) when the same treatment procedure was used. By contrast, bacterial viability was higher for the amino-N-GQDs, N-GQDs, and GQDs without antibody coating than it was for those with antibody coating (23%, 63%, and 88% vs. 0%, 42%, and 65%, respectively). Moreover, for the GQD-based materials with $Ab_{TasA}$ coating, the observed bacterial viability was further reduced, with nearly all bacteria being killed, when a high laser irradiation power was used; nevertheless, the same effect was not observed for the amino-N-GQD, N-GQD, and GQD materials without antibody coating (22%, 36%, and 55% viability, respectively; Figure 2C and Supplementary Information, Figure S4). Although the amino-N-GQDs generated a higher quantity of ROS than did the amino-N-free GQDs and amino-group-free N-GQDs, false-positive ROS signals may have existed; such signals could be caused by interactions among the GQD-based materials, *t*-MVP, XTT, GSH, and SOSG reagent, which could have compromised the PDT results.[18] We recorded the quantities of $^1O_2$ and $O_2.^-$ produced by the laser-irradiated material, namely $Ab_{TasA}$-treated *B. subtilis* (Supplementary Information, Table S3). The quantity of ROS generated by the amino-N-GQD–$Ab_{TasA}$-treated *B. subtilis* was higher than that generated by the N-GQD- and GQD–$Ab_{TasA}$-treated *B. subtilis*; these results were consistent with the ROS results obtained from the determination assay (Supplementary Information, Table S3) and with the measured $\psi_\Delta$ values. The materials without antibody coating (Supplementary Information, Table S4) generated a higher quantity of ROS than did those with $Ab_{TasA}$ coating. This finding demonstrates that $Ab_{TasA}$ successfully coated the materials, resulting in enhanced specificity and selectivity. In summary, the three types of GQD material–$Ab_{TasA}$ facilitated PDT by generating $^1O_2$ and $O_2.^-$ after laser exposure, and material–reagent interactions were not responsible for this effect. These findings are consistent with the trends presented in Figure 2B and C, Figures S5 and S6, and Tables S2–S4 (Supplementary Information), suggesting that bacteria were eliminated through the generation of ROS signals. On the basis of the study findings, we demonstrate that heterocyclic aromatic compounds can be obtained by replacing C atoms with N atoms in $sp^2$-bonded molecular systems. Therefore, such replacement is an effective method for modifying the inherent properties, such as the electronic properties and both surface and local chemical characteristics, of C-based materials. Moreover, the chemical composition of amino-N-GQDs with remarkable quantum confinement and edge effects can be altered to enhance the electrochemical, electrocatalytic, and photochemical activities of such materials, which offers additional benefits in the fields of biomedicine and optoelectronics.[8] The amino-N-GQD-induced increase in ROS observed in the present study may have been caused by the amino-N-GQDs having more frequent intersystem crossing and a higher triplet state yield than did the amino-group-free N-GQDs and amino-N-free GQDs, which led to the amino-N-GQDs having higher PDT-regulated antimicrobial activity.

## TEM and Physiological Assay

We conducted HR-TEM to obtain images of the material-treated bacteria after laser exposure. To determine the most effective ROS generation rate in PDT, we first performed HR-TEM on the amino-N-GQDs. Incubating bare *B. subtilis* (Figure 3A) with amino-N-GQD–$Ab_{TasA}$ for 3 h (Figure 3B; GQD–$Ab_{TasA}$ treatment and N-GQD–$Ab_{TasA}$ treatment (Supplementary Information, Figure S7A and B) had no bactericidal effects (Figure 2B)) resulted in the adsorption of a substantial amount of material on the surface of the bacteria; this could be attributed to the $Ab_{TasA}$ antibody's highly specific binding ability. An uptake assay revealed that approximately 76% of the material was adsorbed onto the bacterial surface within the first 3 h of incubation (Figure 4A), and the rate of adsorption was constant from the 3rd hour to the 12th hour because all adsorption sites on the material were occupied. The physiological functions of bacteria are maintained through ion filtering and nutrient assimilation by the cell wall. However, any adsorbed material acts as a barrier on the surface of bacteria. In this study, the material–$Ab_{TasA}$-treated *B. subtilis* did not exhibit any exceptional morphology after 3 h of incubation; however, after 3 days of incubation, the morphology began to change (Figure 3C), with the estimated viability being 68% (Figure 4B and Supplementary Information, Figure S8). The bacteria could not function normally and died. The amino-N-GQDs adsorbed and coated on the surface of the bacteria hindered the absorption of nutrients crucial for microbial growth and affected cell wall permeability, thereby inhibiting the growth of the bacteria and causing an internal osmotic imbalance. Consequently, after 3 days of incubation, the materials exhibited bacteriostatic or bactericidal capabilities. By contrast, the photoexcited material–

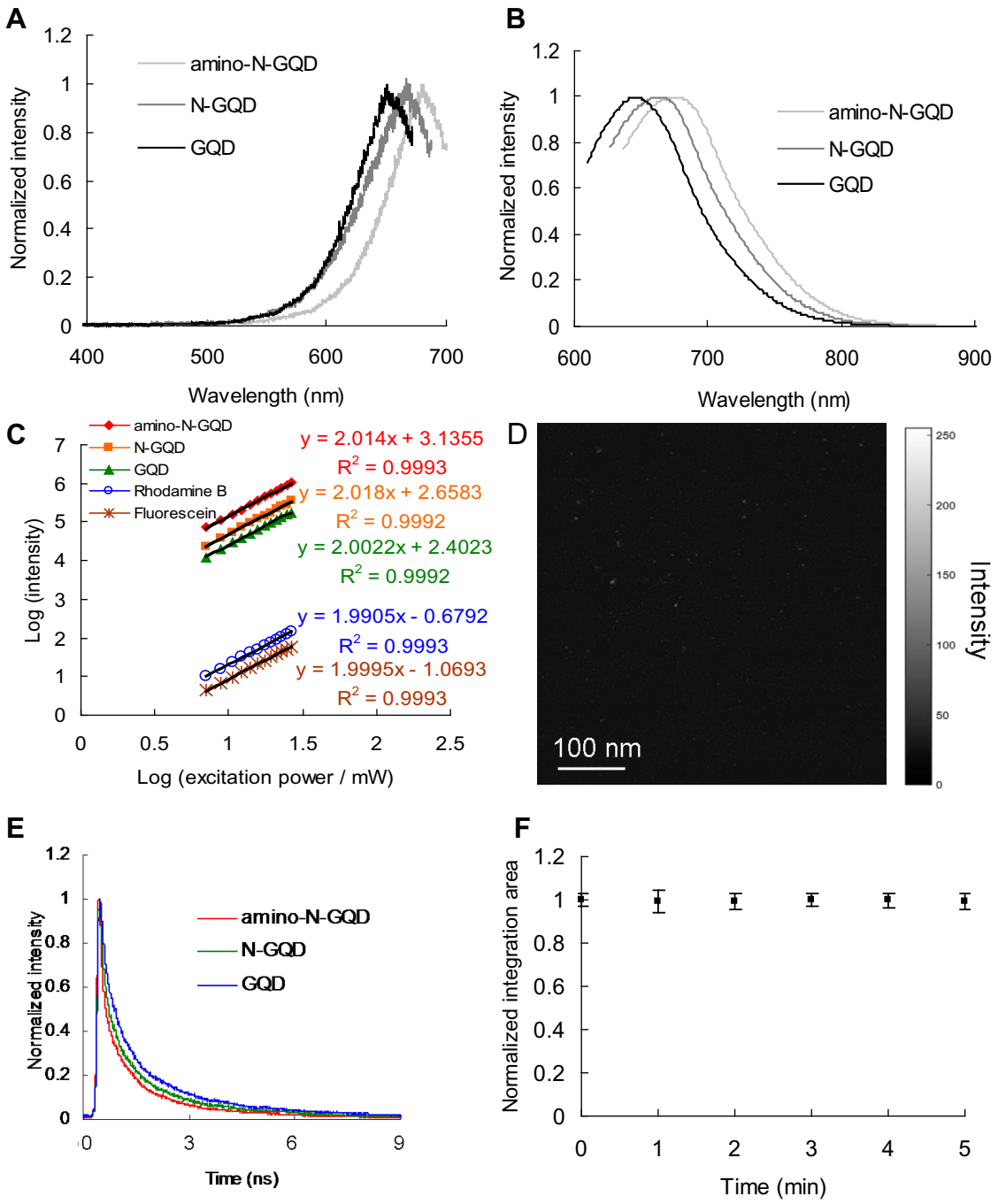


**Figure 5** Relative PL spectra of the materials for (**A**) TPE (98.56 nJ pixel$^{-1}$; cut-off of 700 nm, as determined through cascading filters) and (**B**) OPE (Ex/Em: 630/678 nm, 620/667 nm, and 600/650 nm for the amino-N-GQDs, N-GQDs, and GQDs, respectively). (**C**) Dependence of the TPL intensity on the materials and fluorophore excitation power (logarithm), with the corresponding slopes being approximately 2.00–2.02. The TPE power was 704.0–2816.0 nJ pixel$^{-1}$, and $R^2$> 0.999. (**D**) TPI (gray level) of the amino-N-GQDs at a TPE of 105.6 nJ pixel$^{-1}$ (scanning frequency, 100 scans; total effective exposure time, approximately 0.453 s; scan rate, 4.53 ms scan$^{-1}$; scan area, 200 μm × 200 μm). (**E**) Time-resolved room-temperature TPL material decay profiles at room temperature (105.6 nJ pixel$^{-1}$). (**F**) Two-photon stability of amino-N-GQDs subjected to a TPE power of 566.72 nJ pixel$^{-1}$ for 5 min. The emission intensities of the integrated area after photoexcitation were divided by those of the newly prepared materials without photoexcitation to obtain the normalized integrated area. The TPE wavelength was 800 nm, and delivered material dose was 6 μg mL$^{-1}$. The data are represented as means ± standard deviation (n = 6).

$Ab_{TasA}$-treated *B. subtilis* were severely damaged after 3 h of incubation and exhibited an abnormal morphology (Figure 3D; GQD–$Ab_{TasA}$-treated *B. subtilis* and N-GQD–$Ab_{TasA}$-treated *B. subtilis* (Supplementary Information, Figure S7C and D) exhibited 42% and 65% viability, respectively (Figure 2B)); these results indicate the achievement of nearly 100% bacterial elimination (Figure 2B and C).

## Two-Photon Property and Stability

Because the PL mechanism may involve both intrinsic and defective state emissions,[7] the amino-N-GQDs may have potential for use as a highly effective contrast probe for TPE bioimaging. In general, the average laser power is low under TPE, and the excitation wavelength can be extended to the NIR region, which would enhance the TPL intensity. The TPL intensity, which is a nonlinear phenomenon, increases linearly with the quantum yield (QY), square of the excitation power, and TPE cross section.[3] A large TPE cross section is preferred during the monitoring of molecular actions. Enhanced localized excitation power and intrinsic fluorophores can boost TPL signals under conditions of a high QY and large TPE cross section. In this study, the TPL spectrum of the amino-N-GQDs under TPE (800 nm) revealed a peak at approximately 680 nm (Figure 5A); this peak corresponded to that in the one-photon emission (OPE) spectrum (~678 nm; Ex: 630 nm; Figure 5B). Subsequently, a two-photon process was confirmed; the PL intensity in this process was quadratically dependent on the TPE power (eg, 800 nm),[3] and the corresponding exponent was approximately 2.01 (Figure 5C). Moreover, the two-photon imaging (TPI) emissions of the amino-N-GQDs occurred through a two-photon process (Figure 5D). We estimated the relative QY to be 0.36 (reference QY: 0.28 for Cy5.5 in dimethyl sulfoxide[20]); similarly, the absolute QY[21] was 0.34. The QY values were the same under OPE and TPE.[12] The N-GQDs and GQDs exhibited relative QY values of 0.23 and 0.21, respectively, and absolute QY values of 0.12 and 0.11, respectively. Radiative electron–hole pair recombination was induced by $NH_2$ groups present on the amino-N-GQD surface, and this recombination resulted in the enhancement of intrinsic state emissions. However, a previous study suggested that $NH_2$ groups existing at the edges of N-GQDs possess the highest occupied molecular orbital due to the strong orbital interaction with primary amines.[10] Therefore, the resonance between the delocalized π orbital and molecular orbital existing in the primary amines may have caused orbital band gap narrowing, leading to an increase in the PL QY. Figure 5A presents the TPL spectra. Under TPE at 800 nm, the derived spectra of the amino-N-GQDs, N-GQDs, and GQDs revealed peaks at 680, 669, and 651 nm, respectively. The wavelengths of these peaks were similar to those of the peaks in the OPE spectra (Figure 5A and B). When two-photon techniques are used in vitro or in vivo to investigate and monitor molecular activities, chromophores with large absolute TPE cross sections are particularly desirable because they engender a high absorbed energy–to–input energy flux ratio for a specimen, which reduces the likelihood of photodamage. For the amino-N-GQDs synthesized in this study, we calculated the absolute TPE cross section to be 54,013 Goeppert–Mayer units (GM; 1 GM = $10^{-50}$ $cm^4$ s $photon^{-1}$). Moreover, the absolute TPE cross sections of the N-GQDs and GQDs were approximately 51,628 and 48,379 GM, respectively (Figure 5C, Table 1, and Supplementary Information, Table S5). Rhodamine B served as a reference[20] in the calculations of TPE cross sections. Thus, the absolute TPE cross section was more than three orders of magnitude larger for the amino-N-GQDs than for the traditional fluorophores, and the TPE cross section of the amino-N-GQDs was larger than that of semiconductor quantum dots (Table 1).[12] We measured the lifetime of the materials and sequentially determined the effects of radiative and nonradiative decay rates on the lifetime and QY of the materials (Figure 5E and Table 2). The average lifetime of the amino-N-GQDs was nearly 1.092 ns, which was calculated from the following lifetimes: 0.164, 0.898, and 3.307 ns. The N-GQDs and GQDs had average lifetimes of 1.300 and 1.432 ns, respectively (Table 2). Therefore, the radiative–to–nonradiative decay rate ratio of the amino-N-GQDs was 0.563 (radiative and nonradiative decay rates: $3.297 \times 10^8$ and

**Table 1** TPE Cross Section of Materials (Ex: 800 nm)

| Reference | Integrated emission intensity (counts) | | Action cross-section (ησ) |
|---|---|---|---|
| **Rhodamine B[a]** | **288.61** | | **154.2** |
| **Sample** | **Integrated emission intensity (counts)** | **Relative quantum yield (η)** | **Absolute cross-section (σ)** |
| amino-N-GQD | 36393.651 | 0.36 | 54012.729 |
| N-GQD | 22224.708 | 0.23 | 51627.516 |
| GQD | 10865.882 | 0.12 | 48378.983 |
| Alexa Fluor 594 | 38.603 | 0.66[b] | 31.250 |
| 605 Qdot ITK Carboxyl quantum dots (Q21301MP) | 62386.567 | 0.78[b] | 42733.600 |

**Notes:** [a]Rhodamine B was selected as the standard reference for the cross section, and the relevant calculations are presented in the Materials and Methods. [b]Information was obtained from the official website of Thermo Fisher Scientific (Waltham, MA, USA).

**Table 2** Lifetime Data and Parameters Generated Using a Time-Correlated Single-Photon Counting Technique Involving a Triple-Exponential Fitting Function for Monitoring the Emission at a Wavelength of 800 nm Under TPE

| | 3 exp fitting model: (a0*exp(a1x)+a2*exp(a3x)+a4*exp(a5x)+a6) | | | | | | | lifetime1 | lifetime2 | lifetime3 | average lifetime (ns) |
|---|---|---|---|---|---|---|---|---|---|---|---|
| | a0 | a1 | a2 | a3 | a4 | a5 | a6 | | | | |
| amino-N-GQD | 560.624 | -6.08982 | 875.994 | -1.11307 | 311.320 | -0.30240 | 8.29483 | 0.164208 | 0.898416 | 3.306933 | 1.091904112 |
| N-GQD | 471.662 | -4.54648 | 709.702 | -0.96423 | 232.055 | -0.23264 | 1.53496 | 0.219950 | 1.037096 | 4.298542 | 1.299876050 |
| GQD | 563.053 | -4.36590 | 895.292 | -0.96340 | 333.936 | -0.22151 | 1.52171 | 0.229048 | 1.037992 | 4.514571 | 1.431611057 |

$5.861 \times 10^8$ $s^{-1}$, respectively). The radiative–to–nonradiative decay rate ratios of the N-GQDs and GQDs were 0.299 (radiative and nonradiative decay rates: $1.769 \times 10^8$ and $5.923 \times 10^8$ $s^{-1}$) and 0.136 (radiative and nonradiative decay rates: $8.380 \times 10^7$and $6.145 \times 10^8$ $s^{-1}$), respectively. These findings indicate that after TPE, the materials mainly passed through the radiative pathway when the QY increased and lifetime decreased. The enhanced two-photon properties of the amino-N-GQDs could be attributed to the dots' strong quantum confinement, strong electron-donating effect, highly symmetric band gap, and large π-conjugated systems, which could improve the efficiency of intramolecular charge transfer.[9] Furthermore, the amino-N-GQDs exhibited two-photon stability, as revealed by the dots' post-TPE TPL intensity, resulting in decreased photobleaching (Figure 5F).

## Deep and Noninvasive TPI

We successfully incorporated the amino-N-GQDs into PDT and imaging processes to evaluate their therapeutic effects and demonstrate their potential for use in PDT, which involves the simultaneous elimination and tracking of target bacteria. The amino-N-GQDs had higher relative and absolute PL QY values than did the N-GQDs and GQDs. As illustrated in Figure 6A, a strong emission peak was observed at 680 nm (TPE: 800 nm) in the PL spectrum of the amino-N-GQDs. In addition, the photoexcited amino-N-GQDs were more stable against light than the conventional

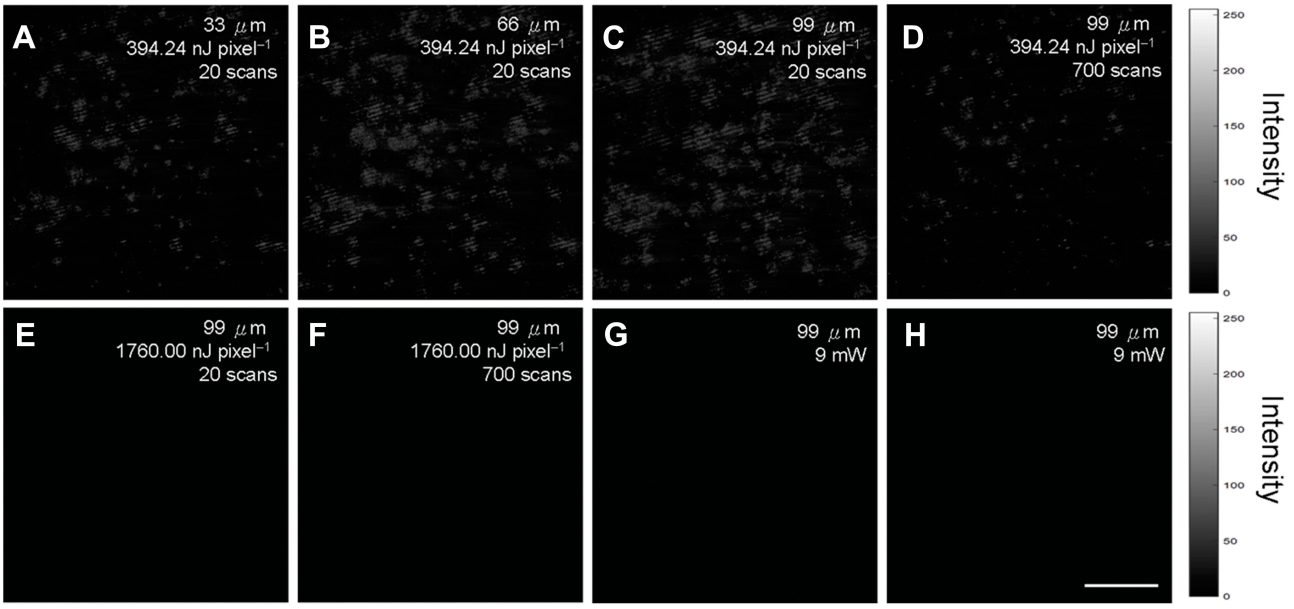


**Figure 6** (**A**–**C**) TPI (gray level) at different depths ranging from 33 to 99 μm for *B. subtilis* at a TPE power of 394.24 nJ $pixel^{-1}$ (20 scans). (**D**) Image acquired after an additional 700 scans. TPAF images of the unlabeled bacteria at a depth of 99 μm and TPE power of 1760.00 nJ $pixel^{-1}$with (**E**) 20 scans (total effective exposure time, ~0.091 s) and (**F**) 700 scans (total effective exposure time, ~3.171 s). The excitation wavelength was 800 nm. One-photon imaging of (**G**) the amino-N-GQD–$Ab_{TasA}$-treated bacteria and (**H**) the unlabeled bacteria following OPE at a fixed output power of 9 mW (Olympus, FV1000, HeNe-R 633 nm, Gas, 40× oil-immersion objective (NA: 1.3) at the same depth). The $OD_{600}$of *B. subtilis* was approximately 0.05, and the delivered dose of material–$Ab_{TasA}$ was 6 μg $mL^{-1}$. The scale bar represents 100 μm.

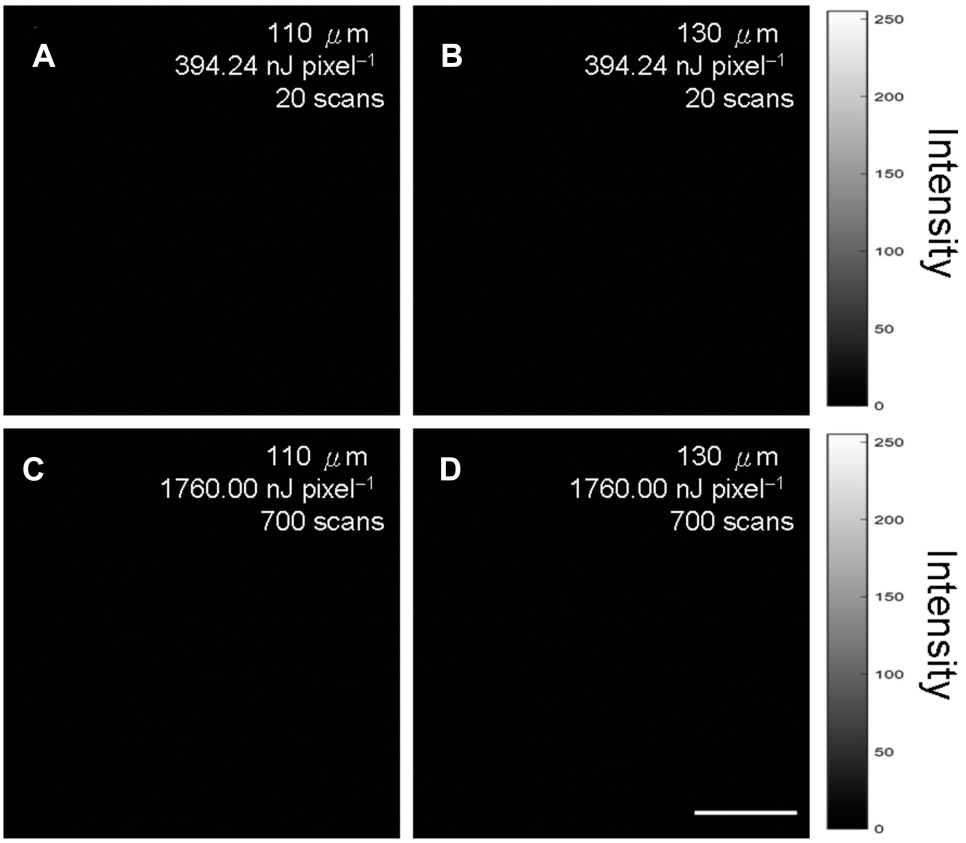


**Figure 7** TPI images (gray level) of (**A** and **B**) the amino-N-GQD–$Ab_{TasA}$-treated *B. subtilis* and (**C**–**D**) TPAF imaging results of the unlabeled cells at different depths ranging from 110 to 130 μm and TPE powers of 394.24 nJ $pixel^{-1}$ (scanning frequency, 20 scans; total effective exposure time, ~0.091 s) and 1760.00 nJ $pixel^{-1}$ (scanning frequency, 700 scans; total effective exposure time, ~3.171 s). TPE wavelength: 800 nm. Delivered dose: $OD_{600}$~0.05 of *B. subtilis* and 6 μg $mL^{-1}$ material–$Ab_{TasA}$. Scale bar: 100 nm.

photosensitizer (Supplementary Information, Figure S9), which resulted in decreased photobleaching. We obtained TPE images of deep tissues by using NIR laser excitation; in this process, we capitalized on the maximum tissue transmission engendered by the amino-N-GQDs as well as on the negligible scattering, relatively low photobleaching, low energy absorption, and optimal irradiation penetration afforded by the NIR region. A 3D biological environment was mimicked by embedding bacteria in a collagen matrix. Figure 6 displays the TPI results obtained after the photoexcitation of layers of GQD-Ab-treated bacteria with various thicknesses (33, 66, and 99 μm). The TPL emitted by the amino-N-GQD–$Ab_{TasA}$-treated *B. subtilis* (Figure 6A–C) at a TPE power of 394.24 nJ $pixel^{-1}$ (Ex: 800 nm), thickness of 99 μm, and scanning frequency of 20 scans revealed bacterial localization, which enhanced the specificity and selectivity of the bound $Ab_{TasA}$ antibodies. We increased the scanning frequency to 700 scans while maintaining the TPE power to execute further photoexcitation for PDT (Figure 7D). We observed that the TPL began to decrease after the additional 700 scans. This finding indicates a change in the bacterial cell wall or oxidation and the ROS-induced deterioration of the surrounding biological surface substrates. These changes may have caused bacterial atrophy, distortion, and morphological damage, revealing that the amino-N-GQDs were desorbed from the surface of the bacteria. Accordingly, the amino-N-GQDs are promising as contrast probes for the monitoring and localization of material-treated bacteria. The amino-N-GQDs can provide information regarding the post-laser-exposure status of bacteria. The lowest TPL intensity was observed when the photoexcitation level was increased. Moreover, in the nontreated bacteria (unlabeled bacteria), two-photon autofluorescence (TPAF) was not easily observed for the intrinsic fluorophores when the TPE power was 1760.00 nJ $pixel^{-1}$ and scanning frequency was 20 scans. Similar results were obtained when the scanning frequency was increased to 700 scans, signifying that the TPI was not compromised (Figure 6E and F). However, we could not observe a one-photon image of the amino-N-GQD–$Ab_{TasA}$-treated *B. subtilis* exposed to a 633-nm laser at a depth of 99 μm (Figure 6G) or an image of the unlabeled bacteria under PDT at the same depth (Figure 6H). Compared

with the OPE wavelength in the NIR region, the OPE wavelength in the visible region exhibited less irradiation penetration and greater energy absorption, photobleaching, and scattering. Therefore, we found it difficult to observe thick tissues and biological specimens. Furthermore, we used TPL and TPAF tissue phantoms to determine the feasibility of conducting imaging processes at specific distances. Imaging processes were feasible at the specified working distance of the lens for both phantoms. TPL images of the material–$Ab_{TasA}$-treated bacteria and TPAF images of the unlabeled bacteria were captured as a function of depth under TPE (Ex: 800 nm). Specifically, the aforementioned images were captured at depths ranging from 110 to 130 μm, with the depth increasing at a rate of 20 μm (Figure 7). TPI emissions were not detected when the TPE power was 394.24 nJ $pixel^{-1}$ (20 scans) or 1760.00 nJ $pixel^{-1}$ (700 scans). Different optical systems have different detection depths. However, the images captured at depths of >100 μm contained spherical aberrations that severely degraded their quality. Such aberrations were caused by a mismatch between the refractive indices of the aqueous sample and immersion oil and were influenced by the objective used, detection efficiency, and maximal *z* depth of the adopted optical laser system. The largest *z* depth observed in this study was approximately 105 μm. This could be attributed to the selected detection efficiency and objective. We suggest that a *z* depth of 99 μm can provide the optimal resolution for examining amino-N-GQDs, which can not only serve as two-photon contrast probes in 3D observations but also eliminate target microbial species.

## Conclusions

This study investigated novel amino-N-GQDs that can not only serve as a photosensitizer but also generate a considerable quantity of ROS. Thus, amino-N-GQDs can be used in alternative PDT approaches involving the elimination of microbes, thus limiting the need for antibiotic treatments. The amino-functionalized N-GQDs generated a higher quantity of ROS than did the amino-group-free N-GQDs and amino-N-free GQDs. Specifically, the amino-N-GQDs conjugated with highly specific antibodies exhibited high antimicrobial activity through a PDT mechanism. The amino-N-GQDs exhibited intrinsic luminescence properties in the NIR region and high photostability, and these properties render them a promising contrast agent for tracking bacteria in 3D bioimaging. Accordingly, amino-N-GQDs offer an alternative method for the observation and easy elimination of malignant microbes. Dual-modality treatment strategies involving amino-N-GQDs could be applied clinically in the future.

## Author Contributions

W.S.K. designed this work, conducted the all experiments. T.S.Y., J.C.L. and C.H.C. conducted the experiments related to biology. C.Y.C. assisted the experiments related to optics & photonics. E.C.S. and P.C.W. designed this work, conducted the experiments related to materials and biology. All authors contributed to data analysis, drafting or revising the article, gave final approval of the version to be published, and agree to be accountable for all aspects of the work.

## Funding

This work was supported by Research Start-Up Fund of Nanjing University of Information Science & Technology, China (2018r047), An Nan Hospital, China Medical University, Taiwan (ANHRF108-19), Ministry of Science and Technology, Taiwan (MOST 108-2314-B-006-053-, 109-2622-E-006-013-CC3, 109-2636-E-006-018-) and the Center of Applied Nanomedicine and Medical Device Innovation Center (MDIC) at National Cheng Kung University from the Featured Areas Research Center Program within the framework of the Higher Education Sprout Project, Ministry of Education, Taiwan. And thanks to the technical services provided by the i-MANI center of National Core Facility for Biopharmaceuticals, Instrument Development Center, Ministry of Science and Technology, Taiwan

## Disclosure

The authors report no conflicts of interest in this work.

## References

1. Xu C, Zipfel W, Shear JB, et al. Multiphoton fluorescence excitation: new spectral windows for biological nonlinear microscopy. *Proc Natl Acad Sci USA*. 1996;93(20):10763–10768. doi:10.1073/pnas.93.20.10763
2. Zharov VP. Ultrasharp nonlinear photothermal and photoacoustic resonances and holes beyond the spectral limit. *Nat Photonics*. 2011;5(2):110–116. doi:10.1038/nphoton.2010.280
3. Albota MA, Xu C, Webb WW. Two-photon fluorescence excitation cross sections of biomolecular probes from 690 to 960 nm. *Appl Opt*. 1998;37(31):7352–7356. doi:10.1364/AO.37.007352
4. Liu Q, Guo B, Rao Z, et al. Strong two-photon-induced fluorescence from photostable, biocompatible nitrogen-doped graphene quantum dots for cellular and deep-tissue imaging. *Nano Lett*. 2013;13(6):2436–2441. doi:10.1021/nl400368v
5. Tian B, Wang C, Zhang S, et al. Photothermally enhanced photodynamic therapy delivered by nano-graphene oxide. *ACS Nano*. 2011;5(9):7000–7009. doi:10.1021/nn201560b

6. Ge J, Lan M, Zhou B, et al. A graphene quantum dot photodynamic therapy agent with high singlet oxygen generation. *Nat Commun*. 2014;5(1):4596. doi:10.1038/ncomms5596
7. Loh KP, Bao Q, Eda G, et al. Graphene oxide as a chemically tunable platform for optical applications. *Nat Chem*. 2010;2(12):1015–1024. doi:10.1038/nchem.907
8. Wang X, Li X, Zhang L, et al. N-doping of graphene through electrothermal reactions with ammonia. *Science*. 2009;324 (5928):768–771. doi:10.1126/science.1170335
9. Trauzettel B, Bulaev DV, Loss D, et al. Spin qubits in graphene quantum dots. *Nat Phys*. 2007;3(3):192–196. doi:10.1038/nphys544
10. Tetsuka H, Asahi R, Nagoya A, et al. Optically tunable amino-functionalized graphene quantum dots. *Adv Mater*. 2012;24 (39):5333–5338. doi:10.1002/adma.201201930
11. Hummers WS, Offeman RE. Preparation of graphitic oxide. *J Am Chem Soc*. 1958;80(6):1339. doi:10.1021/ja01539a017
12. Kuo W-S, Hsu C-LL, Chen -H-H, et al. Graphene quantum dots conjugated with polymers for two-photon properties under two-photon excitation. *Nanoscale*. 2016;8(38):16874–16880. doi:10.1039/C6NR02614A
13. Teng C-Y, Nguyen B-S, Yeh T-F, et al. Roles of nitrogen functionalities in enhancing the excitation-indenpendent green-color photoluminescence of graphene oxide dots. *Nanoscale*. 2017;9(24):8256–8265. doi:10.1039/C7NR01037K
14. Ferrari AC, Basko DM. Raman spectroscopy as a versatile tool for studying the properties of graphene. *Nat Nanotechnol*. 2013;8 (4):235–246. doi:10.1038/nnano.2013.46
15. Kinen MM, Kamal-Eldin A, Lampi A-M, et al. Effects of α- and γ-tocopherols on formation of hydroperoxides and two decomposition products from methyl linoleate. *J Am Oil Chem Soc*. 2000;77(8):801–806. doi:10.1007/s11746-000-0128-z
16. Possel H, Noack H, Augustin W, et al. An oxidant, *tert*-butyl hydroperoxide (TBHP), to serve as a positive control. *FEBS Lett*. 1997;416:175–178. doi:10.1016/S0014-5793(97)01197-6
17. Thompson A, Lever JR, Canella KA, et al. Chemiluminescence mechanism and quantum yield of synthetic vinylpyrene analogues of benzo[*a*]pyrene-7,8-dihydrodiol. *J Am Chem Soc*. 1986;108:4498–4504. doi:10.1021/ja00275a040
18. Lyon DY, Brunet L, Hinkal GW, et al. Antibacterial activity of fullerene water suspensions (nC $_{60}$) is not due to ROS-mediated damage. *Nano Lett*. 2008;8:1539–1543. doi:10.1021/nl0726398
19. Shi L, Hernandez B, Selko M. Singlet oxygen generation from water-soluble quantum dot-organic dye nanocomposites. *J Am Chem Soc*. 2006;128:6278–6279. doi:10.1021/ja057959c
20. Umezawa K, Matsui A, Nakamura Y, et al. Bright, color-tunable fluorescent dyes in the vis/NIR region: establishment of new "tailor-made" multicolor fluorophores based on borondipyrromethene. *Chem Eur J*. 2009;15(5):1096–1106. doi:10.1002/chem.200801906
21. Würth C, Grabolle M, Pauli J, et al. Relative and absolute determination of fluorescence quantum yields of transparent samples. *Nat Protoc*. 2013;8(8):1535–1550. doi:10.1038/nprot.2013.087